

Left Ventricular Function and Perfusion from Gated SPECT Perfusion Images: An Integrated Method

Tracy L. Faber, C. David Cooke, Russell D. Folks, Johnathan P. Vansant, Kenneth J. Nichols, E. Gordon DePuey, Roderic I. Pettigrew and Ernest V. Garcia

Division of Nuclear Medicine, Emory University School of Medicine, Atlanta, Georgia; and Division of Cardiology, St. Luke's-Roosevelt Hospital of Columbia University, New York, New York

A new technique for computing left ventricular function, including left ventricular volumes, mass and ejection fraction, has been developed. This method is a logical extension of the results of a standard perfusion quantification technique; thus, it allows integration of perfusion and functional information. **Methods:** Anatomically based models of the endocardial and epicardial surfaces are generated using the myocardial samples for which perfusion values are quantified, for all frames in the cardiac cycle. With these surface points, left ventricular chamber volume and myocardial volume can be computed. A computer simulation was used to determine the sensitivity of the approach to the assumptions of the model. Validation of volume, mass and ejection fraction was performed with correlative MR studies, and ejection fraction and left ventricular volumes were further investigated using correlative first-pass studies. **Results:** Automated processing was successful in 96% of the cases analyzed. End diastolic volume, end systolic volume, left ventricular mass and left ventricular ejection fraction correlated with MRI with $r = 0.97$, 0.99 , 0.87 , and 0.85 , respectively. Ejection fraction from tomography correlated with first-pass values with $r = 0.82$, and end diastolic and end systolic volumes from tomography correlated with first-pass values with $r = 0.85$ and $r = 0.91$, respectively. **Conclusion:** The new integrated approach is accurate and robust for computing both perfusion and function from perfusion tomograms.

Key Words: gated SPECT; ejection fraction; myocardial perfusion imaging; left ventricular function

J Nucl Med 1999; 40:650–659

It is commonly accepted that left ventricular (LV) functional parameters can be accurately calculated from gated myocardial perfusion tomograms. Various approaches dating from 1986 have been reported for calculating end diastolic (ED) and end systolic (ES) volumes and ejection fraction (EF) from SPECT images. Two primary methods are used.

Geometric approximations can be used with various image measurements to estimate ED and ES volumes or EF (1–5). The most common form of this approach uses boundaries defined on horizontal long axis (HLA) or vertical long axis (VLA) sections to measure axes that can be used with an ellipsoidal LV model. The advantage of this approach is that boundary detection in single slices can be performed rapidly by using a count threshold as a first approximation and by allowing additional processing or user interaction to adjust the edges. Volumes can be computed by using the orthogonal HLA and VLA boundaries as the short axes of ellipsoids, whose volumes can be computed and added together using Simpson's rule. If only a single HLA or VLA slice is used, the length-volume formula can be applied to estimate ED and ES volumes and EF. Another geometrical approach combines a derived formula using conservation of mass with an ellipsoidal LV to relate EF to a single thickening measurement (4). In addition, a mean LV radius computed by averaging the centers of mass of many radial profiles through the myocardium has been used with a spherical volume estimation to compute LV volumes and, thus, EF (5).

The second approach is to perform actual three-dimensional surface detection to provide a more accurate measure of volumes. An early method used maximal changes in image intensity as an initial estimate of edge location, and then modified those boundaries on the basis of an a priori model of LV shape (6). More recently, a method has been introduced that fits Gaussian-shaped functions to profiles of myocardial intensity; the inflection points of the Gaussian are taken to be the surface points (7). This technique also includes checks and constraints to ensure reasonable LV boundaries.

In this article, we describe a new modeling method that estimates the three-dimensional LV endocardial and epicardial surfaces in gated perfusion tomograms for all frames throughout the cardiac cycle. From these boundaries, LV volumes at ED and ES, myocardial mass and EF can be calculated. A computer simulation is used to evaluate the sensitivity of volumes and EF to errors in the modeling

Received Feb. 19, 1998; revision accepted Aug. 28, 1998.

For correspondence or reprints contact: Tracy L. Faber, PhD, Division of Nuclear Medicine, Emory University Hospital, 1364 Clifton Rd., NE, Atlanta, GA 30322.

assumptions. Boundary point accuracy, volumes, mass and EF are validated using correlative 99m Tc-sestamibi SPECT and MR images from 10 patients with myocardial infarction. EF is further validated by comparing the SPECT values with first-pass values in 79 patients.

MATERIALS AND METHODS

SPECT Acquisition and Reconstruction

For all studies, SPECT perfusion imaging was performed using 99m Tc-sestamibi acquired with a GE 400ACT rotating gamma camera (General Electric Medical Systems, Milwaukee, WI) equipped with a low-energy, high-resolution collimator. Studies were performed at rest after intravenous injection of 296 MBq 99m Tc-sestamibi; 3 h later, stress studies were performed after injection of 814 MBq 99m Tc-sestamibi. Sixty-four projections over 180° were acquired for both rest and stress studies; however, stress studies were performed in an electrocardiographic-gated mode using a frame rate of eight frames per cardiac cycle. The closest possible circular orbit was used; the acquisition matrix size was 64×64 pixels with a pixel size of 6.37 mm.

Projections were prefiltered using a two-dimensional Butterworth filter with critical frequency of 0.4 cycles/cm and order of 5 for rest studies and with critical frequency of 0.52 cycles/cm and order of 2.5 for stress studies. Filtered backprojection with a ramp filter was then performed. Reconstructions were reformatted into short-axis slices; the axes used for this reformatting were set manually using software provided by the clinical system.

Perfusion Quantification

The perfusion quantification methods have been described in detail elsewhere (8); they are therefore only summarized here. New automated procedures, however, are discussed in depth. These include automatic identification of the LV apex, base and long-axis center and the radius of a circular region centered about the long axis that encloses the LV in every short-axis slice. In addition, the LV valve plane is detected as two connected planes: one perpendicular to the LV long axis in the lateral half of the LV, and one angled plane in the septal half of the LV. This two-piece valve plane is shown in Figure 1. This definition of the valve plane was adopted because it was judged qualitatively to fit the data well. More important, the dual-plane approach preserves the flat portion, perpendicular to the long axis, which is a necessary part of the

coordinate system defined by the perfusion quantification algorithm.

The automatic processing begins by identifying the apex, a flat basal valve plane and the long-axis center of the left ventricle and a radius of search in which the myocardium can be entirely enclosed. This procedure operates on the volumetric set of short-axis slices as follows: A heart candidate cluster is identified by iteratively raising a threshold from 50% of the maximum image intensity until the isolated object closest to the center of the three-dimensional image is both greater than 40 mL and symmetric within each slice. If no such object can be found, the inferior boundary of the search space is iteratively adjusted superiorly with a threshold fixed at 50% until the isolated object closest to the anterior left corner of the short-axis volume is symmetrical within each slice. This may aid in separating gut activity from myocardial activity. If either of these two operations succeeds, all non-LV clusters are deleted from the image before additional processing. Otherwise, the next steps are performed on the original image in its entirety. The short-axis slices are summed together, excluding the one fifth most apical and the one fifth most basal slices. Within the summed slice, an LV center and myocardial radius are determined such that a majority of points in the slice that survive a 50% of image maximum threshold are *radius* pixels away from an *xcenter* and *ycenter*. This effectively fits a least-cost circle to the threshold data.

A myocardial *cylinder* is defined by extending the detected myocardial circle (center and radius) through each slice of the short-axis volume. The maximal intensity of the volumetric image within the myocardial cylinder is determined. The base is considered to be the first slice basal to the center slice that does not contain (within the myocardial cylinder) a pixel greater than 65% of the maximum. The apex is considered to be the first slice apical to the center slice that does not contain a pixel greater than 40% of the maximum.

Because these parameters that describe the LV limits (LV center, radius, apex and base) may still be in error, they are iteratively adjusted by sampling what is expected to be the myocardium and by recomputing them on the basis of those samples. The sampling is performed on the SPECT short-axis slices using a hybrid cylindrical-spherical coordinate system. The center of the coordinate system is the LV long axis, and the search space is limited by the LV radius, apex and base. Short-axis slices from the basal and medial portion of the LV were sampled using cylindrical coordinates with the cylindrical axis set at the LV long axis; these radial samples were 9° apart. The apical hemisphere was sampled using spherical coordinates; radial samples were taken at the same angular increments as in the cylindrical coordinate system and vertical samples were taken approximately every 12° . The dividing point between the two coordinate systems was patient specific; the distance of this point from the apical point was set to the average radius of all short-axis slices for the patient. The returned sample at each angle was the location of the maximum count value along the radius of that angle, within a searching boundary limit set at three pixels beyond the myocardial cylinder radius.

From the locations of the maximal detected points, new estimates for LV center, base, apex and search radius were computed. The LV center was refined by taking the center of mass of the myocardial samples in the basal three fourths of the LV; the search radius was recomputed as the median of the radii of each myocardial point from the new center plus two pixels. The apex and base were recomputed using two methods. One estimate for the apex was determined as the location of the most apical myocardial

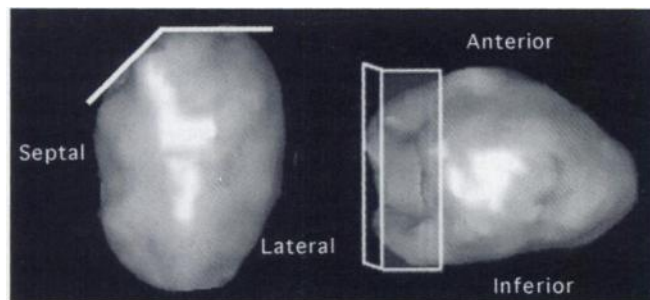


FIGURE 1. Two-plane valve plane. Flat plane perpendicular to LV long axis is fit to lateral half of LV. Angled plane is fit to myocardium in septal half of LV. These planes intersect at line at long axis. Anterior view shows flat plane following lateral basal region and angled plane following septal valve region. Septal view shows transparent two-plane valve plane.

samples within the six most apical angles in the spherical coordinate system. The second estimate was considered to be the first slice apical to the center slice in the short-axis volume that did not contain a pixel greater than 40% of the maximum value within the myocardial cylinder described by the most recent center and radius parameters. If both apex estimates were within one pixel of each other, then the former estimate was kept as the latest candidate. If there was disagreement between the two estimates and if the myocardial sample associated with the first estimate was below 25% of the maximum myocardial counts, then an apical defect was assumed and the latter estimate was used.

The first estimate for the flat, horizontal base plane was determined by finding the mean z value, or slice, in which the sampled myocardial intensity fell to 30% of the maximum sampled counts. The second base estimate was considered to be the first slice basal to the center slice in the short-axis volume that did not contain a pixel greater than 65% of the maximum value within the myocardial cylinder as defined by the latest center and radius values. If the two base estimates differed by less than 2.5 pixels, the former estimate was used; otherwise, a basal defect was assumed, and the latter estimate was assumed to be the more accurate one. Finally, the angled septal portion of the valve plane, coincident with the lateral, flat valve plane, was fit using least-squares minimization to the x, y and z points of the first samples that fell below 30% of the maximum at each angle within the 180° septal range.

The latest refined values for center, radius, apex, base and plane coefficients were compared with the previous ones. If any of the new values were different from the previous values by more than .25 pixel, then all were iteratively recalculated by resampling the image data using each successive set of the most recent parameters. When the parameter estimate stabilized, a final myocardial sampling was performed for perfusion quantification and LV boundary estimation. This final myocardial sampling detected perfusion values at a constant number of radial angles (40) about the LV long axis and at a variable number of vertical samples along the long axis, depending on the number of short-axis slices considered in the cylindrical coordinate system. The detected count values, along with the locations of where each was found, were saved for further processing. The short-axis slice corresponding to the flat base plane was used for the basal limit of perfusion quantification; this maintains the perfusion quantification algorithm as it was originally developed. The center points of the coordinate systems were also saved, so that transformations between the hybrid coordinate system and the original Cartesian coordinate system of the image were straightforward.

Anatomically Based Model of Left Ventricular Boundaries

To create the anatomically based model of the LV boundaries, the radial lengths describing the location of the quantitated perfusion values were considered to be a two-dimensional function of the radial sampling angles and the vertical samples (along the long axis). The quantitated intensity values are the points of maximum intensity within the myocardium. These points should occur at the center of the imaged myocardium because of the SPECT point-spread function (PSF). The SPECT PSF also implies that accurate endocardial and epicardial boundary detection cannot be performed unless the myocardium is thicker than the FWHM, which is typically 1.2–1.5 cm (9,10). For this reason, the myocardial center points are used as a basis to estimate and model

endocardial and epicardial boundaries. By making an assumption that the myocardium is approximately 10 mm thick at ED, the endocardial and epicardial boundary points could be estimated by subtracting and adding 5 mm to all radii in the ED frame to move the endocardial surface in from the myocardial center and to move the epicardial surface out from the myocardial center. This assumption of a 10-mm-thick ED myocardial thickness is well supported in the literature (11–13) and is considered in depth in the Discussion section.

Wall thickening throughout the cardiac cycle was computed using a Fourier analysis of the size-intensity relationship (14). Late-frame drop-off was corrected by scaling all samples in the final frame so that their sum was equal to the sum of all sampled counts in the first frame. For each quantitated perfusion sample, a time-intensity curve was created, and its Fourier transform was computed. The phase and amplitude of the first harmonic of the transform was used to calculate percent thickening (with respect to the ED frame) for all frames in the cardiac cycle. Because the myocardial thickness at ED was presumed to be uniformly 10 mm, the percent thickening information could be used to approximate "absolute" myocardial thickness at each sampled point in the LV, at every gated frame. Once again, endocardial and epicardial boundary points could be determined by subtracting and adding one half of the myocardial thickness to the myocardial center points, respectively. These operations resulted in a set of endocardial and epicardial surface points, corresponding to each quantitated perfusion sample, for all frames in the cardiac cycle. The modeling procedure is shown in Figure 2.

The perfusion analysis was used to determine when myocardial samples were likely to be noise instead of myocardium because of missing counts associated with scarring. Any region of the myocardium containing counts less than 30% of the maximum at ED was considered a likely scar, and all points in this region were pinned to their location at ED. This prevented apparent wall motion associated with incorrect myocardial wall localization in unper-

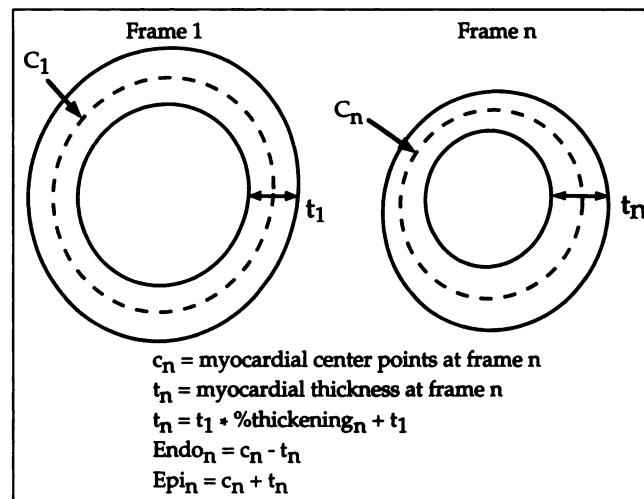


FIGURE 2. Anatomically based model. At ED, myocardial wall thickness is assumed to be uniformly 10 mm thick (t_1). Percent thickening, determined by Fourier analysis, is used with baseline value of 10 mm at ED to predict myocardial thickness at every additional frame in cardiac cycle. For every frame, half of myocardial thickness is added to myocardial center points to create epicardial (Epi) surface points; half is subtracted to create endocardial (Endo) center points.

fused regions. This is discussed more fully in the Discussion section.

For each frame, the two-dimensional function of radii was postprocessed using a two-dimensional 7×7 median filter to remove any extreme, incorrect values. Then a 3×3 smoothing filter was applied to create a surface that better approximated the smoothness of the LV surface. Finally, these radii were converted back into the Cartesian coordinate locations of the endocardial and epicardial surface points, which could be connected together into triangles. Then, the volumes of the resulting polygons associated with endocardial and epicardial surface triangles could be easily computed. Edge points beyond (i.e., more basal than) the angled septal valve plane and their corresponding polygons were excluded from all further LV volume and mass calculations. After this adjustment, the volume enclosed by the endocardial surface points was the endocardial chamber volume. The difference between epicardial and endocardial volumes was the myocardial volume; myocardial mass was obtained by multiplying the volume by a density of 1.05 g/mL. Finally, EF was calculated using ED and ES volumes.

Validations

Computer Simulation. The assumption of ED myocardial thickness used in the model necessitated a study to determine the limits of accuracy of the technique. LVs were simulated in software as truncated ellipsoids with inner (endocardial) and outer (epicardial) surfaces, as seen in Figure 3. The ED axes of the ellipsoids were varied to change ED endocardial volume and myocardial thickness. The ES axes were varied to simulate myocardial motion and myocardial thickening and, ultimately, to vary the ES volume. An abnormal "infarct" region was modeled to move and thicken differently from the rest of the LV; it could also have a different initial thickness from the rest of the "normal" LV.

Two primary abnormal situations were investigated with this simulation. The first modeled overall myocardial hypertrophy in which the ED myocardial thickness was greater than the assumption

of 10 mm; it ranged from 12 to 20 mm. Various ED and ES volumes were modeled using various ED and ES ellipsoidal axis lengths along with different percent thickening values. The second situation modeled the case of an LV aneurysm that could have an ED thickness less than 10 mm (5–10 mm), while the rest of the "normal" myocardium could be thicker than 10 mm (10–20 mm). This aneurysm could also thicken and move differently from the rest of the LV; thus, both myocardial thinning and dyskinesis could be effectively modeled. In all cases, it was assumed that percent thickening was measured accurately.

Using these parameters, simulated LV ED volumes ranged from 22 to 420, and ES volumes ranged from 10 to 351. Myocardial mass ranged from 37 to 318 g. The hypertrophic portions of the LV had an initial thickness ranging from 12 to 20 mm. The aneurysm had an initial thickness ranging from 5 to 9 mm. "Normal" parts of the LV had thickening values ranging from 10% to 55%; aneurysm regions had thickening ranging from 0% to –50% (thinning). The aneurysm size varied from 10% to 55% of the entire LV area. Overall, these parameter variations resulted in more than 750,000 simulations with EF values ranging from 0.10 to 0.87. These actual EF values were calculated using the known actual LV boundaries of the simulation; in addition, a model-based EF was computed by using the assumption of a uniform 10-mm-thick myocardium at the ED frame. Error values in EF were computed by subtracting the model-based measurements from the known true values.

Comparison with MRI. MR images of 10 patients (age range 34–77 y; mean age 59 y) with known or suspected ischemic heart disease were obtained within 48 h of each patient's radionuclide examination using a cine multislice gradient-echo technique (echo time = 6–8 ms, flip angle = 30°, gated to each heart beat) with a Philips 1.5-T ACS scanner (Philips Medical Systems, Best, The Netherlands). Six 128 × 128, interpolated to 256 × 256, short-axis slices with a pixel size of 1.37 mm were obtained over the length of the LV; the thickness of each slice was 10 mm with an interslice gap of 1 mm. Electrocardiographic gating of the acquisition resulted in 12–14 frames per cardiac cycle in this population. ED and ES frames were determined visually.

Endocardial and epicardial boundaries in the ED and ES short-axis MR images were traced by hand by an expert blinded to the SPECT results. The tracings of the endocardial margins included the papillary muscles. Approximately 100 points were detected about the endocardial and epicardial surfaces for each short-axis slice. The anatomically based model for computing epicardial and endocardial surface points was then applied to the gated stress sestamibi studies. To account for differences in orientation and location between the SPECT and MR studies, the MR ED LV epicardial surface was registered to the automatically detected SPECT ED epicardial surface, over translations and rotations, using a technique similar to that described by Faber et al. (15). After this linear registration, the newly reoriented MR surface points were saved for processing.

For each study, error measures based on the distances between SPECT and MR surfaces were calculated. This distance was calculated by determining the angular and axial location, in the SPECT model coordinates, of each point of the MR boundary. The radial location of the SPECT model point at this precise location was computed using bilinear interpolation between the two nearest actual angular and axial samples. The error at that point was then calculated as the scalar magnitude distance between the radius of the interpolated model point and the radius of the MR point. This

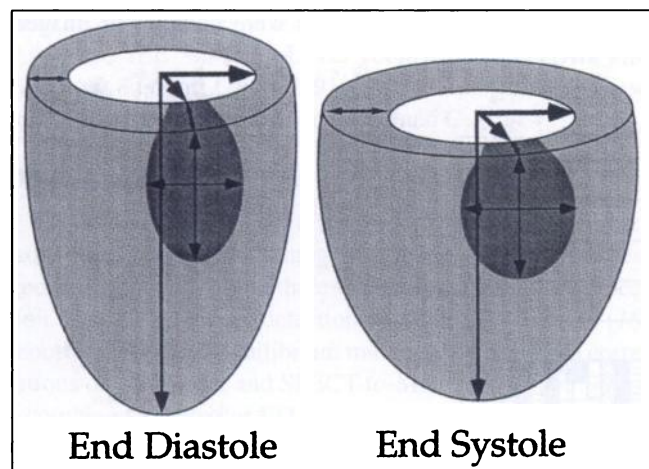


FIGURE 3. Simulation used in computer simulation. Left ventricle was modeled as set of inner and outer ellipsoids, whose radii and centers could be varied. This allowed variations in ED and ES volumes, as well as myocardial thickness and mass. Abnormal "aneurysm" could be included (darker gray region), whose length and width could also be adjusted. Myocardial thickness and radii in aneurysm region were allowed to vary separately from rest of myocardium.

error measure was computed for both endocardial and epicardial surfaces, for both ED and ES.

Global parameters were also validated using the MR studies. ED and ES volumes, myocardial mass and EF computed from the hand-traced MR images were compared with their automatically determined SPECT counterparts.

Comparison with First Pass. We combined patients from two sites in a single analysis to evaluate the accuracy of the anatomically based model for determining EF. Forty-seven patients from Emory University (Atlanta, GA) underwent both ^{99m}Tc -sestamibi SPECT and multicrystal resting first-pass EF evaluations. First-pass studies were performed on the Scinticor-SIM 400 (Scinticor, Inc., Milwaukee, WI), and LV volumes and EF were computed using the SIM 4.04 software available on that system. The EF calculations were performed using automatically generated ED and ES regions of interest (ROIs), except for the valve plane limit, which was designated interactively by the technologist.

An additional 32 patients underwent both perfusion SPECT and function assessment using a validated single-crystal resting first-pass analysis at St. Luke's Roosevelt Hospital (New York, NY). EF from single-crystal first-pass was computed using the methods described by Nichols et al. (16).

EFs were computed from the sestamibi studies using the automatic anatomically based modeling technique. Base, apex, center and search radius parameters were set automatically for all patients; however, these parameters were manually adjusted by a blinded expert if the automatically determined apex or base was judged to be more than two pixels away from where the expert user believed it should have been placed or if the search radius included activity beyond the myocardium. After analysis was complete, EFs from the first-pass analysis were correlated with those from the automatic SPECT methods.

For those first-pass patients who were imaged at Emory, volumes at ED and ES in the first-pass images were calculated using the single-plane geometric technique available on the Scinticor system. ED volume was computed using the two-dimensional geometric approximation of Sandler and Dodge (17) with the ED ROI. ES volume was computed using EF and ED volume: ES volume = ED volume - (EF \times ED volume). These volumes were correlated to those calculated from SPECT with the anatomically based modeling technique.

RESULTS

Computer Simulation

As expected, as ED myocardial thickness increased farther from the assumption of 10 mm, larger errors occurred in the EF. However, even an ED thickness of 20 mm over the entire LV, when the model assumed this thickness to be 10 mm, resulted in less than a 2% mean with a 5% SD error in EF for midsize ventricles. Figure 4 shows EF errors charted against actual mean ED myocardial thickness and ED volume. Note that a bar in this chart may contain examples in which the myocardium was uniformly thicker than 10 mm at ED as well as cases in which thin aneurysms were offset by thicker normal myocardial sections.

Comparison with MRI

For all 10 patients, ED endocardial surface point errors in the SPECT models compared with hand-traced MR images were 3.66 ± 2.21 mm (mean \pm SD); ED epicardial surface point errors were 3.88 ± 2.24 mm. ES endocardial surface point errors were 4.43 ± 2.89 mm; ES epicardial surface point errors were 4.95 ± 3.26 mm. Table 1 lists these errors patient by patient. Figures 5 and 6 show surface points detected in the SPECT images superimposed on both the MR and SPECT images, along with registration results, for two patients.

Globally, the functional variables correlated as follows: ED volumes: $y = 1.11x + 6.48$ mL; $r = 0.97$, SEE = 18.4 mL; ES volumes: $y = 1.04 + 5.94$ mL; $r = 0.99$, SEE = 7.5 mL; mean mass: $y = 1.08 - 4.68$ g; $r = 0.89$, SEE = 23.0 g; and EF: $y = .81x + .093$; $r = 0.88$, SEE = .078. These relationships are charted in Figure 7. In three patients, the basal boundary of the ED LV was not included in the MR field of view. Therefore, these global measures include only those seven patients whose LVs were completely imaged with MRI.

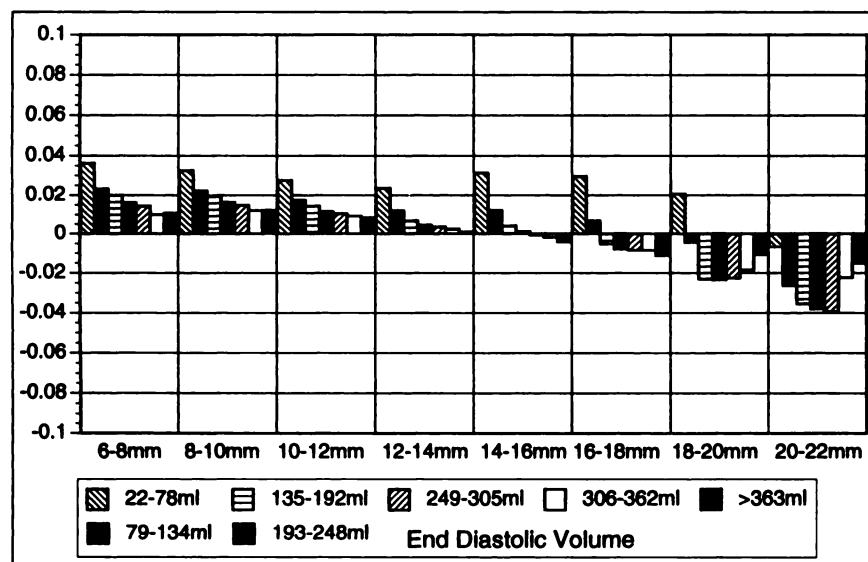


FIGURE 4. Error in EF when mean initial myocardial thickness is different from assumed myocardial thickness of 10 mm. This is charted against mean myocardial thickness at ED and also against ED volume.

TABLE 1
Edge Point Errors Between Hand-Traced Boundaries on MRI and Automatically Determined Edges from Perfusion SPECT

Patient no.	ED endocardial surface			ES endocardial surface		
	Mean	SD	Percentage	Mean	SD	Percentage
1	3.11	1.70	96	4.23	2.61	79
2	3.20	1.78	93	5.87	3.37	61
3	3.14	1.72	94	3.24	1.69	99
4	3.56	2.36	86	3.55	2.46	88
5	3.15	1.92	94	3.51	1.93	91
6	3.99	2.14	84	3.31	1.79	95
7	4.10	2.19	85	4.50	2.80	77
8	4.12	2.47	81	5.08	2.77	69
9	4.40	3.07	81	7.11	4.16	47
10	3.59	1.83	93	3.74	1.80	92

ED = end diastolic; ES = end systolic.

Values are in millimeters. The percentage column indicates the percentage of automatically detected SPECT surface points that are no farther than 6.37 mm (one pixel) from the MR surface.

Comparison with First Pass

Out of the 79 patients studied, the anatomically based model found appropriate initial parameters in 76 patients; this is a 96% success rate. In 2 of the remaining patients, the automatically detected base was set too far apically because of basal defects. In a third patient, the apex was detected too basally, again because of a severe apical defect. After parameters for these three patients were manually adjusted, EFs from all 79 patients correlated as $y = .77x + .108$; $r = 0.82$, SEE = .081. This is shown in Figure 8A.

LV volumes measured using first-pass data from Emory also correlated well with LV volumes computed using gated SPECT. ED volumes correlated as $y = 1.24x + 5.56$ mL; $r = 0.85$, SEE = 43.9 mL. ES volumes correlated as $y = 1.35x + 3.06$ mL; $r = 0.91$, SEE = 28.93 mL. These regressions are shown in Figures 8B and C.

DISCUSSION

Other investigators have derived functional parameters from gated perfusion tomograms using two approaches: geometric modeling and three-dimensional boundary detection. Using a boundary detection approach, Faber et al. (18) reported SPECT-to-equilibrium multigated blood-pool correlations of .93 for EF, and SPECT-to-MRI volumes of .99 for a combined analysis of ED and ES volumes (6). Germano et al. (7), using a more highly automated approach, reported a correlation of .91 when SPECT EFs were compared with first-pass values. Using geometric approximations with manually drawn two-dimensional contours, DePuey et al. (1) obtained EFs from gated SPECT that correlated with equilibrium multigated blood-pool values in a range of 0.79–0.88, depending on the observer. Automation of these techniques (2) demonstrated high correlation of EF with equilibrium gated blood-pool imaging ($r = 0.87$) and first-

pass imaging ($r = 0.87$) with additional improvement of agreement with first-pass EF ($r = 0.90$) achieved by regional image enhancement even among the most severely hypoperfused patients (19). Volumes computed using the same techniques have also been shown to agree well with angiography, with correlations of $r = 0.84$ for ED volume and $r = 0.91$ for ES volume (20). Mochizuki et al. (3) used a geometric approximation with two-dimensional contours to obtain correlation coefficients of 0.92, 0.90 and 0.83 for ED volume, ES volume and EF, when SPECT was compared with contrast ventriculography. The same technique gave values of ED volume, ES volume, EF and myocardial mass that correlated with MRI as $r = 0.99$, 0.96, 0.89 and 0.92, respectively. The geometric approximation of Smith et al. (4) resulted in SPECT EFs that correlated with equilibrium blood-pool radionuclide ventriculography as $r = 0.91$ (21).

Our approach provides similar accuracy to that described in the literature. For the set of 7 patients with myocardial infarction studied with MRI and SPECT, we obtained correlations similar to those reported by Faber et al. (6) and Mochizuki et al. (3). In the 79 patients we studied with SPECT and first-pass ventriculography, we obtained correlations similar to those reported by DePuey et al. (1). The SEE is also an important parameter for evaluating accuracy of quantitative measurements. All published methods of computing EF from gated perfusion SPECT demonstrate similar errors of the estimate (when such statistics are reported) when correlated to first-pass or equilibrium blood-pool values; the SEEs range from 0.069 to 0.081 (2,5,7).

Although the accuracy of this method is comparable with other published approaches, it is important to note the limitations of first-pass radionuclide ventriculography as a gold standard. It is well understood that stress-induced myocardial ischemia can persist for hours. Therefore, both volumes and EF obtained from gated SPECT may not be indicative of the true resting baseline, and EF will in fact be decreased compared with the resting first-pass value (22). In other cases, a high post-stress catecholamine state may induce a higher EF than true resting baseline. Although comparison of heart rates in correlative studies would help to ensure similar physiological states during both studies, heart rate information during SPECT acquisition is not available for the patients in this study. Therefore, differences in physiological states between correlative studies may explain the scatter of EF values around the regression line in Figure 8A. In addition, the calculation of EF from first-pass images is a two-dimensional technique that is dependent on user placement of the atrioventricular valve plane. A loose bolus, improper background subtraction, poor ROI demarcation and misplacement of the valve plane can all affect the accuracy of first-pass EFs. Volume measurements from first-pass are estimated using a two-dimensional geometric model rather than relative counts and are even more susceptible to inaccuracies. We believe MRI is the best correlative study for evaluating function measures obtained

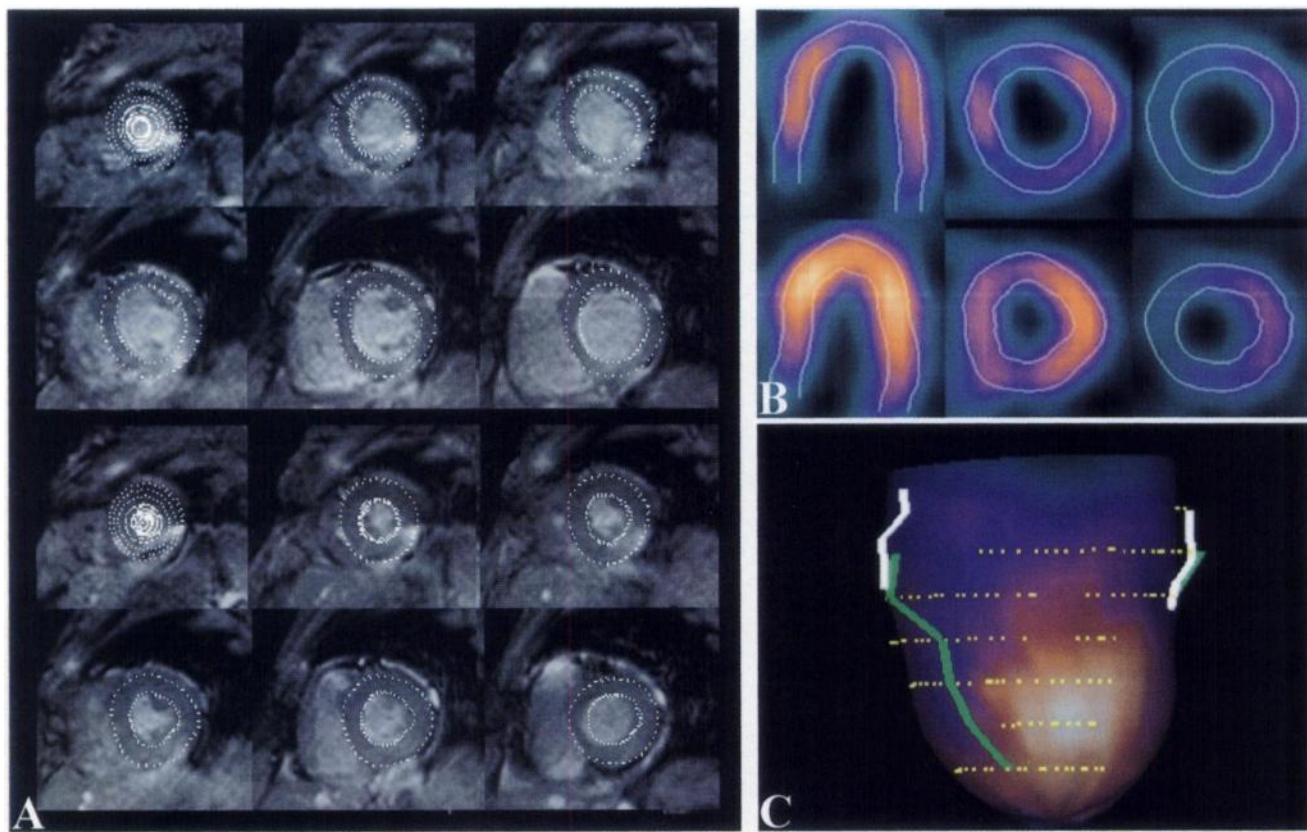


FIGURE 5. Results from functional analysis for patient with anterior infarct. (A, top two rows) ED epicardial and endocardial boundary points computed in gated SPECT study, superimposed on registered MR images. (A, bottom two rows) ES epicardial and endocardial boundaries computed in gated SPECT study, superimposed on registered MR images. (B) Detected boundaries superimposed on SPECT images at ED (top row) and ES (bottom row). (C) Registration results. Epicardial surfaces created from SPECT studies, color coded for perfusion, and endocardial points hand-traced from MR images, in yellow. Interventricular grooves in SPECT study are shown in white; grooves from MR image are shown in green.

from gated SPECT; however, first-pass measures are more frequently obtained and used clinically.

The accuracy of both EF and wall thickening based on 8 gated frames per cardiac cycle, as opposed to 16 frames or more, has been investigated in the past (7,14). Germano et al. (7) demonstrated that the use of an 8-frame study results in a constant and predictable decrease of 0.04 in EF, compared with a 16-frame study. This issue is less important for the MR images used for validation, because they were acquired at 12–14 frames per cardiac cycle, and is completely moot for the first-pass studies, which were acquired dynamically with approximately 32 frames per cardiac cycle. However, there is no inherent reason that the modeling method described here cannot be applied to gated studies having more than 8 frames. We use 8-frame gated stress studies clinically; therefore, validation of parameters computed from clinical studies was of utmost importance.

Of course, it is only possible to *estimate* the myocardial wall location in the case of a large defect caused by myocardial infarction. Nichols et al. (19) demonstrated that in patients having defects below 15% maximum extending through >25% of the myocardium, it is still possible to find reasonable boundaries. Their approach assumes, as does our

method, that the maximal count along each radial sample is in the myocardium. Empirically, we also frequently see very low, but still existing, levels of counts in many severely hypoperfused LV segments. However, when there is no perfusion data (counts) at all, no method can find edges that do not exist in the image. This is particularly problematic when the scarring is apical, and the most apical boundary of the LV cannot be seen. In our approach, we force the wall to be a smooth connection between noninfarcted portions of the wall; this approximation is similar to that used by other methods. In addition, infarcted portions of the myocardium are pinned to their ED positions, so they do not move during the cardiac cycle. The rationale behind this estimation is that when tissue is so damaged as to not be visualized in the image, we can do no better than to estimate that it is smoothly connected to living tissue and that it does not move. In fact, 2 of our MR validation patients (patient nos. 2 and 9) had infarcts covering 25% or more of the LV wall area. The average boundary point error in these patients was slightly larger (by 0.2 mm) than in the other 8 patients. This difference is statistically significant at $P < 0.05$; however, it is certainly not clinically significant. The goodness of

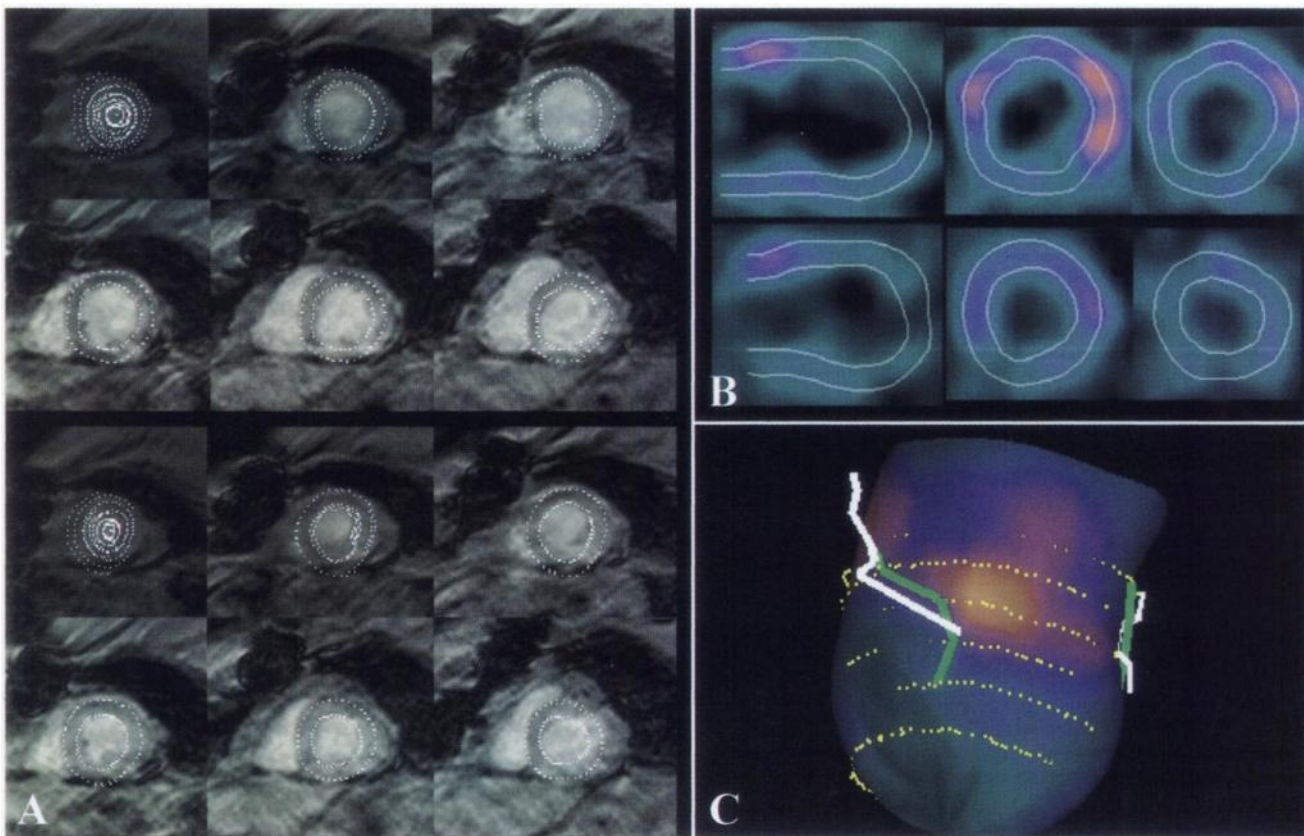


FIGURE 6. Results from functional analysis for patient with apical aneurysm. (A, top two rows) ED epicardial and endocardial boundaries computed in gated SPECT study, superimposed on registered MR images. (A, bottom two rows) ES epicardial and endocardial boundaries computed in gated SPECT study, superimposed on registered MR images. (B) Detected boundaries superimposed in SPECT images at ED (top row) and ES (bottom row). (C) Registration results. Epicardial surfaces created from SPECT studies, color-coded for perfusion, and epicardial points hand-traced from MR images, in yellow. Interventricular grooves in SPECT study are shown in white; grooves from MR study are shown in green.

endocardial boundary estimation in one of these infarct patients can be seen in Figure 6.

The errors seen in EF calculated using perfusion studies of small or hypertrophic hearts are generally attributed to artifactually increased counts in the LV chamber, which are

in turn caused by scatter and the detector response effect (2,23). The resulting change in apparent count distribution decreases ES volume and, therefore, increases EF. However, these inaccuracies are seen primarily with explicit edge detection, when a gradient or threshold operator cannot

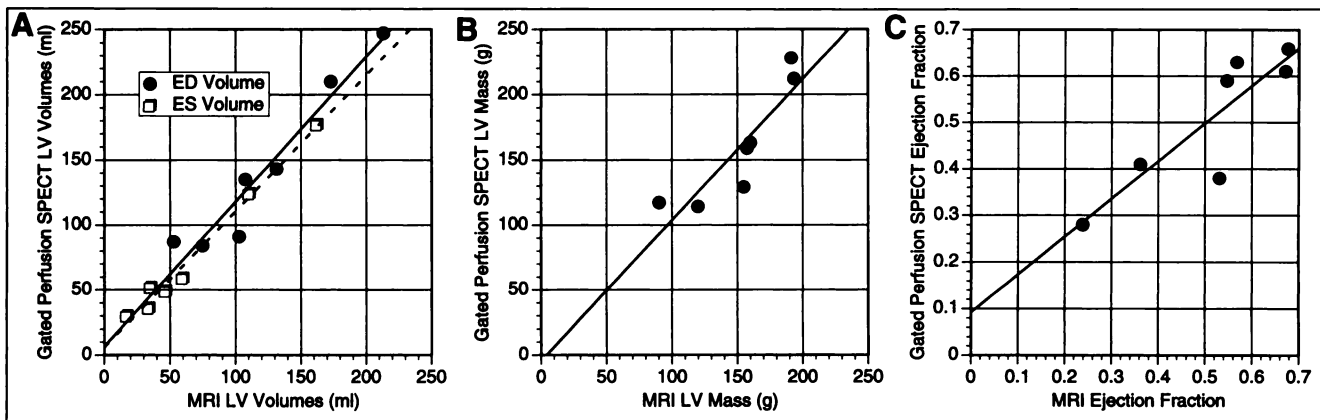


FIGURE 7. (A) SPECT volumes versus MR volumes at ED and ES. ED volumes correlated as $y = 1.11x + 6.48 \text{ ml}$; $r = 0.97$, SEE = 18.4 mL. ES volumes correlated as $y = 1.04x + 5.94 \text{ mL}$; $r = 0.99$, SEE = 7.5 mL. (B) SPECT mass versus MR mass. Mass correlated as $y = 1.08x - 4.68 \text{ g}$; $r = 0.89$, SEE = 23.0 g. (C) SPECT EF versus MR EF. EF correlated as $y = .81x + .093\%$; $r = 0.88$, SEE = 0.078. LV = left ventricular.

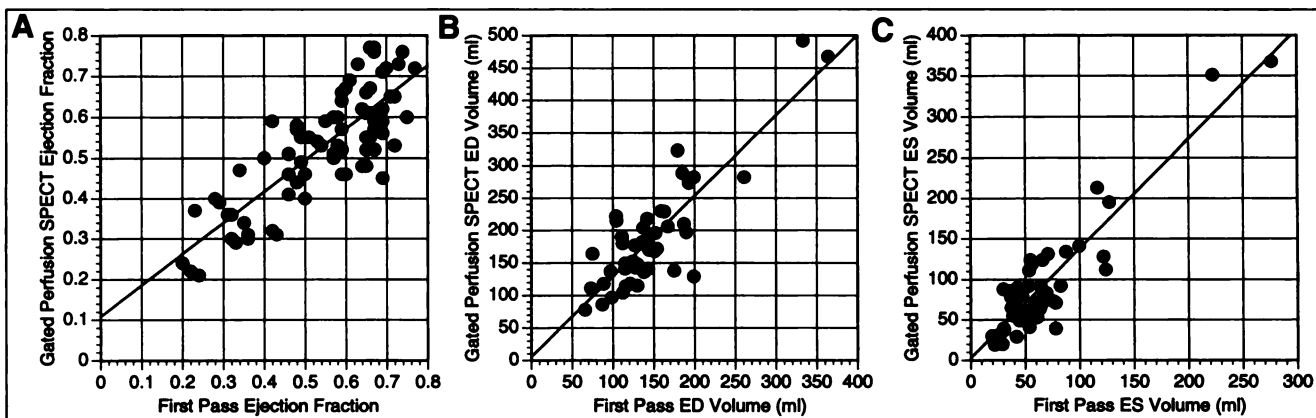


FIGURE 8. (A) SPECT EF versus first-pass EF for 79 patients studied at Emory and St. Luke's Roosevelt Hospital. EF correlated as $y = .77x + .108$; $r = 0.82$, SEE = 0.081. (B) SPECT ED left ventricular volumes versus first-pass volumes for patients studied at Emory. Volumes correlated as $y = 1.24x + 5.56$ mL; $r = 0.85$, SEE = 43.9 mL. (C) SPECT ES volumes versus first-pass for Emory patients. ES volumes correlated as $y = 1.35x + 3.06$ mL; $r = 0.91$, SEE = 28.93 mL.

correctly identify the true wall boundary because of detector response-induced count distribution changes. In this case, our approach is also likely to underestimate ES volume and overestimate EF, because scatter and detector response also affect the position of the maximum within the myocardial count profile. However, the position of the maximal count is changed much less severely than the position of the maximal gradient (24) and, therefore, our method should prove less sensitive to these problems. In contrast, hypertrophy of the myocardium violates the assumption of a 1-cm-thick myocardium at ED. This is a more important factor in assessing accuracy of our method.

This assumption of a 1-cm-thick myocardium at ED is quite valid for normal myocardium. Measurements using MRI have shown the mean ED thickness to be 10.1 ± 1.7 mm over the entire LV (11). Similar values were obtained by Kaul et al. (12). On short-axis MR slices, myocardial thickness ranged from $10.2 \pm .5$ mm at the chordal level of the posterior wall to 10.4 ± 1.8 mm at the papillary muscle level of the septal wall. Also, Byrd et al. (13) found using MRI that ED LV septal and posterior wall thickness was 11 ± 2 mm and 11 ± 1 mm, respectively, in 15 normal adults. Although it is obvious that thickness will be less uniform and farther away from the norm of 10 mm in abnormal patients, MR studies of patients with myocardial infarction have shown the mean myocardial thickness to be very close to our approximation of 10 mm. Pflugfelder et al. (11) evaluated myocardial segments in patients with myocardial infarction on the basis of their perfusion and their observed motion. In this study, normal segments were 10.1 ± 1.7 mm, ischemic but normally moving segments were 12.2 ± 3.5 mm, hypokinetic segments were 9.1 ± 4.7 mm, akinetic segments were 8.5 ± 2.9 mm and dyskinetic segments were 5.0 ± 3.4 mm. However, in most patients, the majority of myocardium is normal, and dyskinetic segments comprise a small portion of the LV. In the study by Pflugfelder et al. (11), the mean myocardial thickness over the entire LV in 15 infarcted patients was 10.44 ± 4.2 mm. Even in those cases

in which a large portion of the myocardium is composed of scar tissue and is therefore thinner than the assumption, our computer simulation indicates that the model-based estimate of EF will be within .03 of the true value for LVs with ED volumes greater than 80 mL. Similarly, when the entire myocardium is 18- to 20-mm thick (instead of our assumption of 10 mm), the model-based estimate will be within .02 of the true value.

Beyond what is known about ED myocardial thickness in normal and abnormal patients, the computer simulation undertaken in this project demonstrates that for the vast majority of patients EF can be reliably estimated using our model. The success rate of 96%, as measured by the number of first-pass patients properly analyzed, is similar to that reported by Germano et al. (25). Note that this success rate is not inclusive of automatic reconstruction limits or reorientation axes, because this work used short axis slices as the starting point.

Even though this modeling approach is similar in accuracy to other methods, most of the previously published approaches have kept quantitative LV functional analysis completely separate from quantitative perfusion analysis. Even though these other methods use perfusion to measure LV function, separate analysis programs are usually required to quantitate perfusion. Therefore, the results of perfusion analysis can only be qualitatively compared with functional analysis. Because LV function and perfusion are intimately related and because they provide complementary information, an integrated system that quantitatively analyzes both is desirable. At least one integrated approach has been described (4), underlining the importance of such a unified system. Our method of LV functional analysis operates entirely within the perfusion quantification framework, using the same coordinate system and display technologies. Thus, we are able to compute, display and compare directly functional information, such as thickening, with perfusion quantification information, such as reversibility. Regional myocardial mass corresponding to normal versus infarcted

tissue can be directly calculated and used to compute mass at risk. Such measurements are increasingly important for treatment planning, cardiac remodeling and prognosis.

CONCLUSION

LV function can be measured accurately from gated perfusion studies by estimating endocardial and epicardial boundaries using a modeling approach that combines structural information obtained from a mature and robust technology for perfusion quantification.

ACKNOWLEDGMENT

This work was funded in part by National Institutes of Health grant no. R01HL42052. The authors receive royalties from the sale of CEqual®, PertSPECTive® and the Emory Cardiac Toolbox® related to the research described in this article. The terms of this arrangement have been reviewed and approved by Emory University in accordance with its conflict-of-interest practice.

REFERENCES

1. DePuey EG, Nichols K, Dobrinsky C. Left ventricular ejection fraction assessed from gated technetium-99m-sestamibi SPECT. *J Nucl Med*. 1993;34:1871–1876.
2. Nichols K, DePuey EG, Rozanski A. Automation of gated tomographic left ventricular ejection fraction. *J Nucl Cardiol*. 1996;3:475–482.
3. Mochizuki T, Murase K, Tanaka H, et al. Assessment of left ventricular volume using ECG-gated SPECT with technetium-99m-MIBI and technetium-99m-tetrofosmin. *J Nucl Med*. 1997;38:53–57.
4. Smith WH, Kastner RJ, Calnon DA, et al. Quantitative gated single photon emission computed tomography imaging: a counts-based method for display and measurement of regional and global ventricular systolic function. *J Nucl Cardiol*. 1997;4:451–463.
5. Everaert H, Franken PR, Flamen P, et al. Left ventricular ejection fraction from gated SPET myocardial perfusion studies: a method based on the radial distribution of count rate density across the myocardial wall. *Eur J Nucl Med*. 1996;23:1628–1633.
6. Faber TL, Stokely EM, Peshock RM, et al. A model-based four-dimensional left ventricular surface detector. *IEEE Trans Med Imaging*. 1991;10:321–329.
7. Germano G, Kiat H, Kavanagh PB, et al. Automatic quantification of ejection fraction from gated myocardial perfusion SPECT. *J Nucl Med*. 1995;36:2138–2147.
8. Garcia EV, Cooke CD, Van Train K, et al. Technical aspects of myocardial SPECT imaging with Tc-99m sestamibi. *Am J Cardiol*. 1990;66(suppl):23E–31E.
9. Galt JR, Garcia EV, Robbins WL. Effects of myocardial wall thickness on SPECT quantification. *IEEE Trans Med Imaging*. 1990;9:144–150.
10. Eisner RL, Boyer AS, Dunn D, et al. Inherent limitations in wall thickness and mass measurements from SPECT myocardial perfusion scans [abstract]. *J Nucl Med*. 1989;30:796R.
11. Pfugfelder PW, Sechtem UP, White RD, Higgins CB. Quantification of regional myocardial function by rapid cine MR imaging. *AJR* 1988;150:523–529.
12. Kaul S, Wismer GL, Brady TJ, et al. Measurement of normal left heart dimensions using optimally orientated MR images. *AJR*. 1986;146:75–79.
13. Byrd BG, Schiller NB, Botvinick EH, Higgins CB. Normal cardiac dimensions by magnetic resonance imaging. *Am J Cardiol*. 1985;55:1440–1442.
14. Cooke CD, Garcia EV, Cullom SJ, et al. Determining the accuracy of calculating systolic wall thickening using a fast Fourier transform approximation: a simulation study based on canine and patient data. *J Nucl Med*. 1994;35:1185–1192.
15. Faber TL, McColl RW, Opperman R, Corbett JR, Peshock RM. Spatial and temporal registration of cardiac SPECT and MR images: methods and evaluation. *Radiology*. 1991;179:857–864.
16. Nichols K, DePuey EG, Gooneratne N, et al. First-pass ventricular ejection fraction using a single crystal nuclear camera. *J Nucl Med*. 1994;35:1292–1300.
17. Sandler H, Dodge H. The use of single plane angiograms for the calculation of left ventricular volume in man. *Am Heart J*. 1968;73:325–334.
18. Faber TL, Stokely EM, Corbett JR. Surface detection in dynamic tomographic myocardial perfusion images by relaxation labeling. *SPIE 1001: Visual Communications and Image Processing* 1988:297–301.
19. Nichols K, DePuey EG, Rozanski A, et al. Image enhancement of severely hypoperfused myocardia for computation of tomographic ejection fraction. *J Nucl Med*. 1997;38:1411–1417.
20. Tamis JE, Nichols K, Malhotra S, et al. Comparison of gated SPECT to x-ray contrast angiographic ventricular volume measurements [abstract]. *J Am Coll Cardiol*. 1997;29:482A.
21. Calnon DA, Kastner RJ, Smith WH, et al. Validation of a new counts-based gated single photon emission computed tomography method for quantifying left ventricular systolic function: comparison with equilibrium radionuclide angiography. *J Nucl Cardiol*. 1997;4:464–471.
22. Johnson LL, Verdesca SA, Aude WY, et al. Postischemic stunning can affect left ventricular ejection fraction and regional wall motion on post-stress gated sestamibi tomograms. *J Am Coll Cardiol*. 1997;30:1641–1648.
23. Case JA, Cullom SJ, Bateman TM, Barnhauf C, Saunders MJ. Overestimation of left ventricular ejection fraction by gated MIBI myocardial perfusion SPECT in patients with small hearts [abstract]. *J Am Coll Cardiol*. 1998;31(suppl A):43A.
24. Faber TL, Akers MS, Peshock RM, Corbett JR. Three-dimensional motion and perfusion quantification in gated single-photon emission computed tomograms. *J Nucl Med*. 1991;32:2311–2317.
25. Germano G, Kavanagh PB, Berman DS. An automatic approach to the analysis, quantitation and review of perfusion and function from myocardial perfusion SPECT images. *Int J Cardiac Imaging*. 1994;13:337–346.